

The Beta Problem: A Study of Abell 262

James D. Neill¹

Astronomy Department, Columbia University, New York, NY 10027

neill@astro.columbia.edu

Jean P. Brodie

Lick Observatory, University of California, Santa Cruz, CA 95064

brodie@ucolick.org

William W. Craig¹ and Charles J. Hailey

Columbia Astrophysics Laboratory, Columbia University, New York, NY, 10027

bill@astro.columbia.edu

chuckh@astro.columbia.edu

and

Anthony A. Misch

Lick Observatory, University of California, Santa Cruz, CA 95064

tony@ucolick.org

ABSTRACT

We present an investigation of the dynamical state of the cluster A262. Existing optical line of sight velocities for select cluster galaxies have been augmented by new data obtained with the Automated Multi-Object Spectrograph at Lick Observatory. We find evidence for a virialized early-type population distinct from a late-type population infalling from the Pisces-Perseus supercluster ridge. We also report on a tertiary population of low luminosity galaxies whose velocity dispersion distinguishes them from both the early and late-type galaxies. We supplement our investigation with an analysis of archival X-ray data. A temperature is determined using *ASCA* GIS data and a gas profile is derived from *ROSAT* HRI data.

¹Visiting Astronomer, Lick Observatory. Lick Observatory is operated by the Regents of the University of California.

The increased statistics of our sample results in a picture of A262 with significant differences from earlier work. A previously proposed solution to the “ β –problem” in A262 in which the gas temperature is significantly higher than the galaxy temperature is shown to result from using too low a velocity dispersion for the early-type galaxies. Our data present a consistent picture of A262 in which there is no “ β –problem”, and the gas and galaxy temperature are roughly comparable. There is no longer any requirement for extensive galaxy-gas feedback to drastically overheat the gas with respect to the galaxies. We also demonstrate that entropy-floor models can explain the recent discovery that the β values determined by cluster gas and the cluster core radii are correlated.

Subject headings: galaxies: clusters: individual (Abell 0262) – galaxies: clusters: general – X-rays: galaxies

1. INTRODUCTION

Clusters of galaxies provide an opportunity to study the formation of massive structures through gravitational accretion. The cluster dark matter potential well is an environment in which infalling and virialized galaxies interact with intra-cluster gas in a complex, time-dependent fashion involving dynamical friction with dark matter as well as galactic winds and ram-pressure stripping. Measurements of cluster galaxies and gas temperatures as a function of radius, element abundances, luminosity-temperature relations and the evolution of these quantities with redshift all provide data to test theories of cluster formation and evolution. Clusters also provide a probe of many cosmological parameters. The density of clusters forming as a function of redshift can be used to measure quantities such as Ω_0 and the spectrum of density perturbations in the early universe.

One problem which arises in exploring the topics described above is the β –problem. Assuming that gas and galaxies are both tracers of the dark matter potential well, and that no source of energy other than gravity is operative, there is a relation between the ratio of the internal energy of the galaxies and the gas temperature (determined using spectroscopic data and generally termed β_{spec}) to a quantity related to the gas and galaxy density profiles (determined by fitting isophotes to the X-ray gas and optical emission and generally termed β_{fit}). The failure of these two quantities to agree in most clusters was noted some time ago (Sarazin 1986). Numerous solutions have been offered over the years. These include adjustments of β_{fit} to properly account for the galaxy distribution as indicated by galaxy-galaxy correlation measurements (Bahcall & Lubin 1994); galaxy velocity distribution asymmetries (Menci & Fusco-Femiano 1986); incorrect determinations of β_{spec} due to contamination of velocity dispersions by cluster substructure (Edge & Stewart 1991b); and presence of significant galaxy-gas feedback or dynamical friction with dark matter (Bird, Mushotzky, & Metzler 1995, hereafter BMM95). David, Jones, & Forman (1996, hereafter DJF96) have proposed that the β –problem is solved by excluding late-type galaxies when estimating the cluster velocity dispersion since such galaxies are still infalling and therefore not virialized.

The β -problem is significant for several reasons. The measurement of β from X-ray and optical data provides information about the nature of galaxy-gas feedback. It is complementary to other methods used to probe the galaxy-gas interaction such as heavy element abundance gradients. The β -problem will become increasingly important as more accurate cluster temperatures become available from *Chandra* and *XMM*. With improved temperature measurements, β uncertainty, which appears in the conversion from gas temperature to mass in the Press-Schechter formula (Press & Schechter 1974), can contribute significantly to the mass uncertainty. It is essential to confirm that the gas dynamic-dark matter simulations are correct, since they are utilized to obtain β . In fact, the comparison of β values derived from modeling with those obtained from optical observations indicate marginal agreement given the observational and theoretical uncertainties (Henry 1997).

Many problems can lead to a cluster violating the assumptions required for β_{spec} to equal β_{fit} . These problems include use of non-virialized galaxy populations, use of galaxies associated with infall or other peculiarities in the velocity field, local sub-clustering, presence of cooling flows or magnetic fields etc.. There are several approaches to evaluating the possibilities. The first approach is to observe many clusters, with the number of spectra collected per cluster generally limited to ~ 20 or less, and to statistically analyze the resultant data. With adequate temperatures and substructure analyses the calculation of “average” cluster properties may then represent a “typical” member of the sample population, with any scatter being random. As a complement to this statistical approach, an analysis of individual clusters through use of extensive X-ray and optical data permits correction for many effects and thus provides an alternative testbed for comparison with both theory and the results of the statistical approach. Such detailed analyses are rare because they require much high quality optical and X-ray data. We are obtaining large numbers of redshifts for several clusters for eventual comparison with *XMM* and *Chandra* data.

In this paper we describe a detailed investigation of A262. We augmented existing galaxy redshift data with a sample of new redshifts obtained with the Automated Multi-Object Spectrograph at Lick Observatory. We have also analyzed previously unpublished *ROSAT* and *ASCA* data. The complete data set allows us to address the problems discussed above.

2. OBSERVATIONS & INITIAL ANALYSIS

We combined new observations of A262 with published redshifts to produce the sample from which we derived cluster optical properties. Here we describe the new observations, compare our data to published data, and discuss the generation of a uniform catalog. We also present our analysis of the X-ray data to derive the profile and temperature of the X-ray gas. We use $H_0 = 65$ $\text{km s}^{-1}\text{Mpc}^{-1}$ in our analysis.

2.1. AMOS Observations

The Automated Multi-Object Spectrograph (AMOS, Craig et al. 1993) consists of a robotic fiber positioner at the prime focus of the Lick 3m telescope, a fiber feed, and a floor-mounted spectrograph. Sixty fibers (39 more are planned) can be positioned within a 1° field of view to an accuracy of 0.1 arcsecond. Constraints on the fiber placement typically limit the number of fibers that can be assigned to objects and the unassigned fibers are used to monitor the sky background. We used the red channel of the spectrograph with the 700 line/mm grating giving a spectral resolution of $0.7 \text{ \AA}/\text{pixel}$ over the range $6200 - 7500 \text{ \AA}$.

A preliminary target list of galaxies brighter than ~ 18.5 in V within A262 was generated from a 1° -square Digitized Sky Survey image centered on the cluster. Our goal was to improve the velocity sampling within the virial radius of the cluster. We used two AMOS pointings, offset by only 18 arcminutes, to improve the density of targets selected within this region. Final target selection by the fiber placement algorithm results in a random spatial sampling of this region. Combining our observations with previously published velocities ensures that spatial biasing of the cluster is minimized. Figure 1 shows the spatial distribution of our sample and the sample of previously published velocities. The elongation of the cluster in the SW to NE direction has been seen in every study of A262 (see section 3 for references).

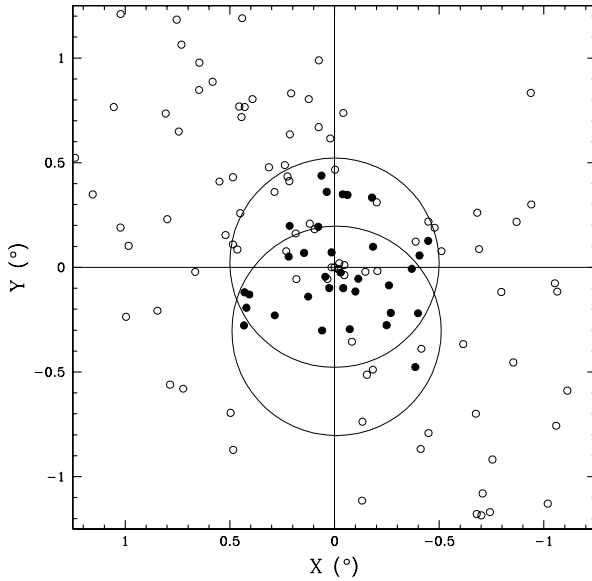


Fig. 1.— The spatial sampling of A262. The two pointings are indicated by the large circles. The smaller filled circles indicate the galaxies observed by AMOS, open circles indicate galaxies with observations from the literature.

Spectra were obtained using AMOS on the nights of 1998 November 19–20. The two pointings

yielded 46 object spectra, 29 with an exposure time of 5400s and 17 with an exposure time of 9000s. Since the spatial overlap for these two pointings is significant, the effect of the differing exposure times on our analysis of the cluster dynamics is negligible. The unassigned fibers monitored the night sky lines during the exposures and were used for the night sky subtraction.

All observations were reduced and analyzed using IRAF (Tody 1986). The SPECRED package was used to extract one-dimensional spectra from the registered and coadded CCD images. A wavelength solution was generated from calibration lamp spectra and was checked against the night sky lines and measured to have an internal error of less than 0.5\AA . We generated a master sky spectrum for each pointing and used the SKYTWEAK task to scale and shift the master sky until the RMS of the object spectra was minimized. We chose to examine each spectrum individually to eliminate spurious velocities due to poor sky subtraction.

The redshift of A262 ($z = 0.016$) puts the H- α absorption feature in a region that is relatively free from night sky lines (6671 \AA). For absorption systems the RVSAO (Kurtz & Mink 1998) task XCSAO was used to cross-correlate with a zero-velocity K giant spectrum from Jacoby, Hunter, & Christian (1984). For emission systems the RVSAO task EMSAO was used with a line catalog that included H-alpha, NII, SII, and OII. Heliocentric corrections were applied to derive the final velocities. As described below, Tonry & Davis (1979) R values, which measure the quality of the cross-correlations, were one of the criteria used for removing spurious velocities before combining with observations from the literature. The error in the velocity is calculated from the width of the cross-correlation peak and the R value (see Kurtz & Mink (1998)) and also contributed to the selection process.

2.2. Redshifts From the Literature

The CfA redshift catalog² (Huchra 1999) formed the basis of our literature catalog. A search for more recent data, not included in the CfA catalog, revealed only the Scoddeggi, Giovanelli, & Haynes (1998, hereafter SGH98) study of early-type galaxies.

Galaxies in common were used to check for systematic offsets between the three catalogs (CfA, SGH98, and ours) prior to combining them. Figure 2 shows the comparison for the absorption line systems in our catalog with both literature catalogs. We calculated the average and standard deviation of the velocity offsets with respect to each of the published catalogs. For the CfA catalog the offset is $4 \pm 259 \text{ km s}^{-1}$ for 15 galaxies in common. The offset for the three common galaxies with the largest R values is $6 \pm 81 \text{ km s}^{-1}$. For the SGH98 catalog we derive an offset of $7 \pm 56 \text{ km s}^{-1}$ with 5 galaxies in common.

We also checked the previously observed emission line galaxies. This comparison is shown in

²available at <http://cfa-www.harvard.edu/~huchra/zcat/>

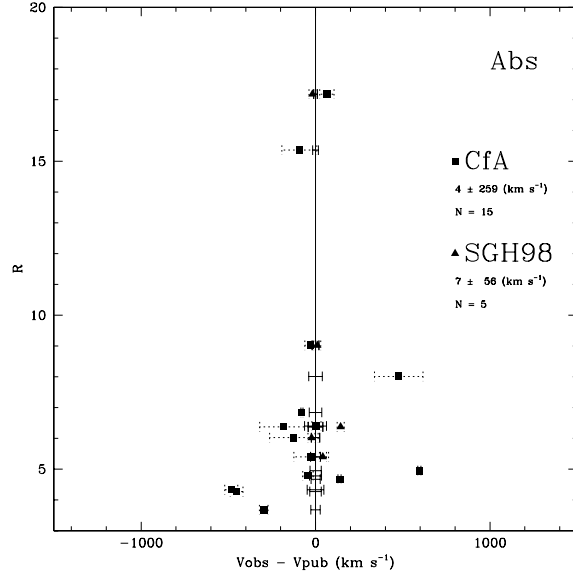


Fig. 2.— A comparison of our velocities with the CfA redshift catalog and SGH98 velocities for absorption line galaxies. Our error bars are plotted along the zero offset line at our measured R value. Solid points indicate the offset from the published value for each previously observed galaxy with the published error indicated by a dashed error bar.

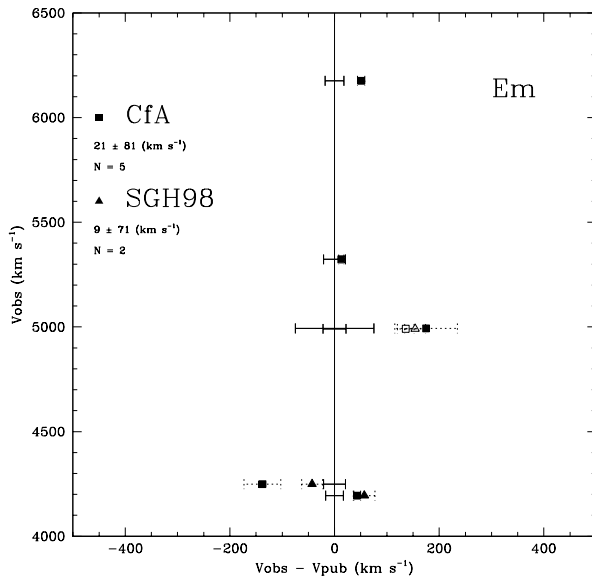


Fig. 3.— A similar comparison to Figure 2 for the emission line galaxies, but with the y-axis being our observed velocity.

Figure 3. The calculated offset for the CfA catalog in this case is $22 \pm 81 \text{ km s}^{-1}$ for 5 galaxies in common. There are only two galaxies in common with SGH98 and these yield an offset of $10 \pm 71 \text{ km s}^{-1}$.

Based on these offsets and standard deviations, we concluded that there is no statistically significant velocity offset between the catalogs. We combined the catalogs into a master catalog of 207 velocities covering A262 out to a radius of 4° . The velocities of galaxies with multiple observations were combined with a weighted average after checking each observation for quality. In the cases where there were three observations, any velocity that disagreed significantly with two velocities that agreed was removed before averaging. In the cases where there were two observations that disagreed significantly, the good observation was chosen to have an R value of greater than 5.5 (see Figure 2) or to have the smaller quoted error. Table 1 lists the new velocities.

The morphologies of our galaxies were derived from their appearance on the Digitized Sky Survey image. Most of the brighter galaxies had previously been classified and we used these classifications whenever possible. The previously unclassified galaxies in our catalog were divided into two broad categories depending on the presence or absence of disk-like structure. This division was refined using the spectroscopic appearance by classifying any galaxy with emission lines as a generic spiral, classifying any disk-like galaxy with no emission lines as an S0, and classifying the remaining non-disk galaxies with no emission lines as generic ellipticals. We checked this classification scheme against the previously classified galaxies and confirmed its accuracy.

50 galaxies, from 15 different sources within the CfA catalog, had no published classification. Of these, 32 have published B magnitudes and average 0.5 magnitudes fainter than the classified galaxies. This unclassified population has interesting properties and will be discussed in sections 3 and 4.

2.3. X-Ray Data

We supplemented our optical data with X-ray data from public archives. We used *ROSAT* HRI data taken on 1996 July 25, *ROSAT* PSPC data taken on 1992 August 10, and *ASCA* GIS2 and GIS3 data taken on 1994 January 22–23. All datasets were downloaded from the HEASARC data archive. We used the HRI data to fit the gas distribution because of its high spatial resolution, and because of A262’s very small core radius ($0.01 \text{ Mpc} \sim 0.4 \text{ arcmin}$).

We examined the *ROSAT* PSPC data to see if we could identify infalling galaxies by their X-ray emission and remove them from the sample. Only 4 of our galaxies had an appreciable count rate in the PSPC image ($> 0.01 \text{ ct s}^{-1}$) and removing these from the sample produced no detectable change in our results.

Figure 4 shows the X-ray contours for the *ROSAT* HRI and Figure 5 shows the X-ray contours for the *ASCA* GIS overplotted on an image from the Digitized Sky Survey of A262. All of the

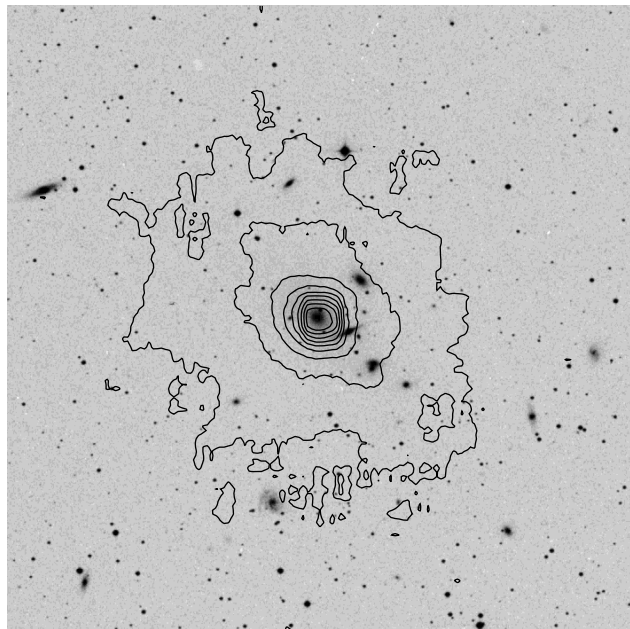


Fig. 4.— X-ray contours for the *ROSAT* HRI overplotted on the DSS image of A262.

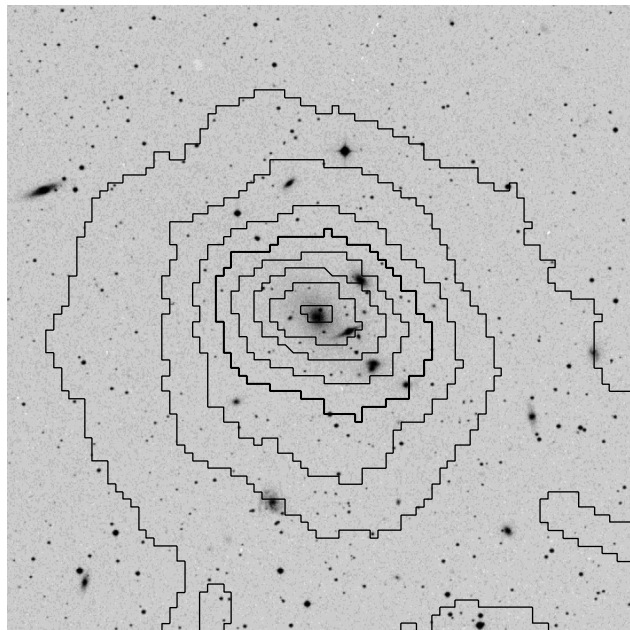


Fig. 5.— X-ray contours for the *ASCA* GIS overplotted on the DSS image of A262.

X-ray images show a centrally peaked, slightly elliptical, smooth profile. None show any sign of bi-modality and all have monotonically decreasing intensity profiles from the cluster center. DJF96 analyzed the PSPC image in detail and discuss the correlation between the X-ray and optical structure. They found that a modified King profile was consistent with the profile for A262.

2.3.1. Profile Fitting

The X-ray gas profile of A262 was fitted using the vignetting-corrected HRI image available from the archive. This image includes data from HRI spectral bands 2 to 10 and has a total exposure time of 14616s. We applied the isophote fitting routine ELLIPSE from IRAF (Jedrzejewsky 1987) and fit from 0–100 pixels (0–13 arcmin) using the geometric bin spacing algorithm which creates larger bins for the lower signal wings and smaller bins in the inner region where the signal is high and the profile is steep. We then fit the isophotal values with a modified King model. Neumann & Arnaud (1999, hereafter NA99) showed that a point source at the center of a cluster can systematically bias $\beta_{fit,gas}$ and recommend a process for fitting the profile that involves removing data points from the center until the reduced χ^2 statistic stops getting smaller. Others have used a similar technique to remove the influence of a central cooling flow (David, Jones, & Forman 1995, hereafter DJF95). Fitting the entire range of data gives a $\beta_{fit,gas}$ of 0.5 ± 0.1 and an X-ray core radius (r_{cx}) of 0.008 ± 0.005 Mpc with a reduced χ^2 of 3.05. Using the technique of NA99 we removed the central 5 points (out to 0.2 arcmin) and fit a $\beta_{fit,gas}$ of 0.6 ± 0.1 with an r_{cx} of 0.009 ± 0.005 Mpc at a reduced χ^2 of 1.07. To test for the influence of the central cD on this profile, we also fit the data after removing the data points out to the core radius (0.4 arcmin). This fit yielded values that agreed within the errors. The agreement of all these values indicates that the influence of a cooling flow or a central point source is small.

DJF95 used PSPC data to derive a $\beta_{fit,gas}$ of 0.53 ± 0.03 which is consistent with our value to within the error bars. The core of A262 would be only partially resolved in the PSPC and this may have produced a lower $\beta_{fit,gas}$. Our r_{cx} also agrees well with the optical core radius (r_{co}) measured by Girardi et al. (1998a, hereafter G98). G98 measure a value of 0.02 Mpc using a modified King profile for the surface density of galaxies in the optical.

We adopt a value for $\beta_{fit,gas}$ of 0.6 ± 0.1 and r_{cx} of 0.009 ± 0.005 Mpc for the remainder of our analysis.

2.3.2. X-ray Temperature

We utilized the *ascascreen* procedure from the HEASARC software archive, with the strict background rejection setting, to filter the raw event files for the two GIS detector data sets. The method outlined by Arnaud (1996) for spatial-spectral fitting was followed. This consists of using XSELECT to extract spectra in annuli centered on the peak emission. We divided the central 12

arcminutes of the image into 4 annuli each 3 arcmin wide. The temperature gradient of A262 reported in DJF95 is consistent with an isothermal profile and we did not attempt to fit temperatures for the individual annuli. The corresponding background spectra were extracted from the standard blank-sky observations covering the same cutoff rigidity range and with the same selection criteria. The XSPEC package (Arnaud 1996) was used to perform the spectral fitting using the *ascac* model which calculates the energy-dependent scattering between annuli given the spatial distribution of the emission. We used our derived profile convolved with the GIS point spread function for the spatial model. For the spectral model we used a Raymond-Smith thermal plasma with photo-absorption and allowed the temperature, abundance, column density and normalization to vary. This produced a temperature for the gas of 1.79 KeV (1.71–1.91 KeV 90% cl) at an abundance of $0.3 \pm 0.15 \text{ Z}_\odot$ and a column density of $6.7 \pm 3.1 \times 10^{20} \text{ cm}^2$ with a reduced χ^2 of 1.01.

We tested for possible contamination from the higher temperature background cluster 20 arcmin to the west of A262 (see DJF96). We performed the same analysis, first dividing the image into a west half and an east half. The derived temperatures for both halves agreed with our previous result to within the errors and we conclude that this background cluster does not affect our analysis.

Our value for the temperature lies between that derived from *ROSAT* PSPC data DJF95; 1.36 KeV (1.21–1.48 KeV 90% cl), and that derived from *Einstein* (David et al. 1993), *EXOSAT* (Edge & Stewart 1991a); 2.4 KeV (2.2–2.7 KeV 90% cl), and *Ginga* (Arnaud & Evrard 1999); 2.41 ± 0.05 KeV. The *Einstein*, *EXOSAT*, and *Ginga* temperatures may be higher because they are contaminated by the background cluster due to their larger fields of view. The limited spectral coverage of the *ROSAT* PSPC (0.2–2.0 KeV) may have biased the analysis of those data to lower temperatures. The *ASCA* GIS has a narrower field of view and good spectral resolution and coverage and so it does not suffer from either biasing or contamination.

An X-ray temperature of $1.79^{+0.08}_{-0.05}$ KeV (1σ) is used for the rest of this paper.

3. DETAILED ANALYSIS

In this section we present the analysis of our redshift catalog to determine the dynamical properties of A262.

3.1. Substructure Tests

We used our expanded catalog of velocities to identify the subpopulation of galaxies within A262 that is the most relaxed and representative of the dark matter potential well. Other studies have examined A262 using all populations and have not found significant substructure (Sakai, Giovanelli, & Wegner 1994; Girardi et al. 1997). Girardi et al. used a multi-scale wavelet analysis

with equally weighted spatial and velocity contributions for a large sample of clusters. They reproduced well-documented substructure in other clusters, but did not detect any in A262.

We find a complex picture emerges when the galaxies are examined by subpopulation. The completeness limit of our catalog (~ 16 in V , determined using the APS database³) does not allow us to draw strong conclusions about substructure from the spatial distribution of the catalog. However, our conclusions from the analysis of the velocities should be much more robust since the galaxies are then simply test-particles in the potential well of the cluster. The distance dimming through the cluster is only 0.1 magnitude so the sampling through the cluster is uniform. We first touch on the picture derived from the spatial distribution of the subpopulations and then examine the velocity data in detail.

Previous studies have noted that A262 has a centrally-concentrated early-type population of galaxies overlaid with a later-type population that is infalling from the Pisces-Perseus supercluster ridge, of which A262 is a member (Sakai, Giovanelli, & Wegner 1994; Moss & Dickens 1977). Figures 6–8 display the spatial distribution of the galaxies with velocities within the range $3500.0 < V_\odot < 6500.0$ km s⁻¹ and the peculiar velocities with respect to the cluster average. Figure 7 shows that the early-type population is centrally concentrated, while in Figure 8 the later-type population is clearly more dispersed.

We present the velocity histograms for four subpopulations of galaxies within the virial radius in Figure 9. We used the ROSTAT algorithm (Beers, Flynn, & Gebhardt 1990) to test each of these histograms for Gaussianity and to derive the average heliocentric velocity and velocity dispersion with errors using the bi-weight estimators which are robust to the presence of outliers.

Table 2 presents the results of this analysis. The last three columns present the Gaussianity test statistics. The first statistic is the scaled tail index (TI, Bird & Beers 1993) which varies from 0.84 for a uniform distribution up to a 1.62 for a Cauchy distribution. A Gaussian distribution has a TI value of 1.0. The early population is closest to Gaussian using this statistic, the late population tends toward the uniform distribution, and the unclassified population is more centrally peaked than a Gaussian, in agreement with the appearance of the histograms in Figure 9. The second and third statistics (the a- and W-tests) are described in Yahil & Vidal (1977). For the a-test an infinite Gaussian distributed sample would have the value 0.7979. Again, the early population is closest to this value. The W-test statistic for a Gaussian has a value of 1.0. The early population has the value closest to 1.0 and also has the highest probability of being drawn from a Gaussian parent population (92%).

As a test for the effects of incompleteness on our conclusions, we isolated a complete subsample of our catalog with $V < 16$ and derived the same statistics. The values were identical within the much larger errors (due to the smaller sample) and we conclude that incompleteness has not effected

³The APS databases are supported by NASA and the University of Minnesota, and are available at <http://aps.umn.edu/>

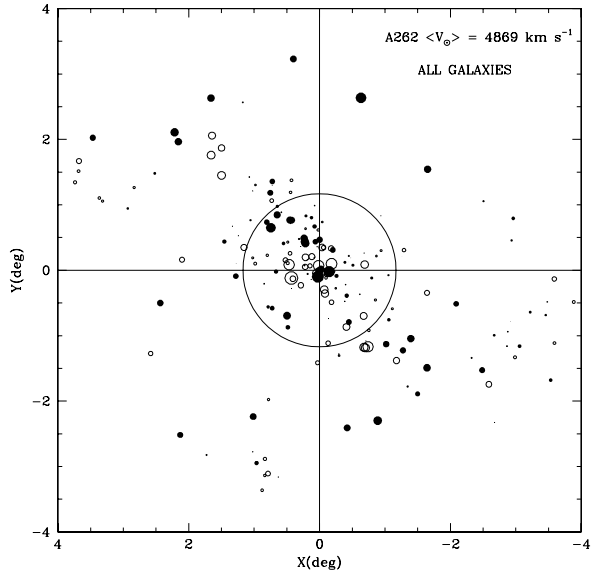


Fig. 6.— The spatial distribution of the entire catalog with peculiar velocities encoded as follows: filled circles represent galaxies with negative peculiar velocities, open circles represent galaxies with positive peculiar velocities, and the size of the circle represents the magnitude of the peculiar velocity. The large circle represents the virial radius of 1.52 Mpc (1°17').

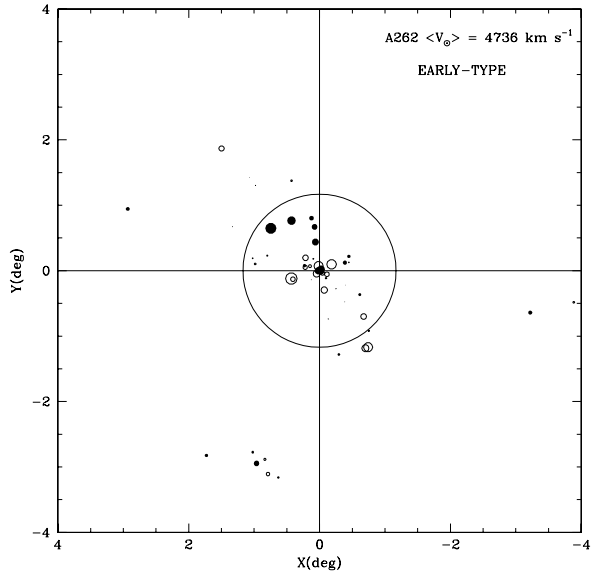


Fig. 7.— As for Figure 6, but for only the early-type galaxies.

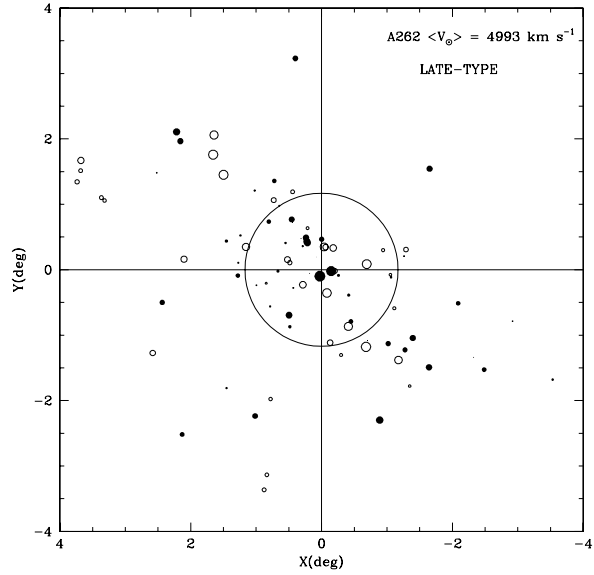


Fig. 8.— As for Figure 6, but for only the late-type galaxies.

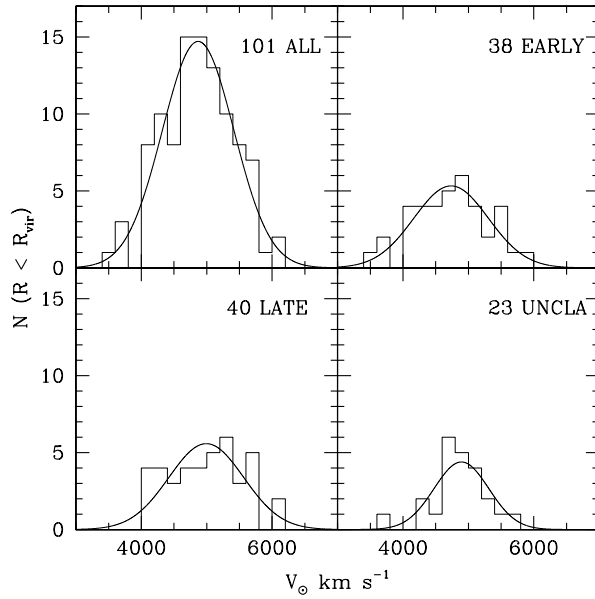


Fig. 9.— The velocity histograms for the subsets of the catalog within r_v with a Gaussian as specified in Table 2 overplotted.

our velocity analysis.

3.2. Average Heliocentric Velocity and Velocity Dispersion Profiles

The average projected integrated heliocentric velocity profiles are presented in Figure 10. The integrated projected velocity dispersion profiles (VDPs) appear in Figure 11. Each point was calculated with ROSTAT as described above for each population and within the radius indicated. The cluster center is defined to be the position of NGC 708, the central cD. There is some evidence that NGC 708 may be slightly offset from the dynamical center of the cluster (see DJF96). We chose not to account for this due to the small magnitude of the offset and the large uncertainty in its value. The values for the entire cluster population, the early and late-type population, and the unclassified galaxies are plotted in the figures. The error bars are the 1σ confidence limits.

Several important features are apparent in these plots. Each population shows an isothermal profile both in the VDP and in the heliocentric velocity. We tested 2nd order polynomial fits against flat fits using reduced χ^2 statistics and found that the flat fits did as well or better than the polynomial fits in each case. There are two offsets that are significant in these plots as well. The early population is offset from the other populations in heliocentric velocity and the unclassified population is offset from the others in the VDP. We tested the significance of these offsets by using a chi-squared fitting technique which explicitly accounts for the fact that the true parameter values for the galaxy populations are unknown, and themselves estimated from the data. The best fit value for the early and late populations have them offset by 260 km s^{-1} . The probability that the early and late type heliocentric velocity profile data is drawn from a common parent population is $< \sim 10^{-5}$. The same analysis was performed to test the reality of the offset of the VDP profile of the unclassified population versus that of the classified galaxy population. The unclassified population VDP is offset from the classified population VDP by 230 km s^{-1} and the chance that the two data sets are drawn from a common parent population is $< \sim 7 \times 10^{-4}$. The VDPs for the late and early type galaxy populations are statistically indistinguishable.

The spatial distribution of the unclassified population is presented in Figure 12. These galaxies cannot be considered relaxed, despite their lower velocity dispersion, since they have a very dispersed spatial distribution, more like the late-type galaxies in Figure 8.

The profiles and spatial distributions are consistent with the previous studies of A262 described above. The isothermal VDP, centrally concentrated spatial distribution, and Gaussianity tests confirm that the early-type population is relaxed. If infall of the unclassified population occurs along the supercluster ridge, which is coincident with the plane of the sky, this could explain their low velocity dispersion.

Table 2 presents the derived properties out to r_v for the four population samples of our catalog. We consider only the early-type population to be relaxed and will use their values for the remaining analysis. It can be seen from Table 2 that the influence of the late-type population on the velocity

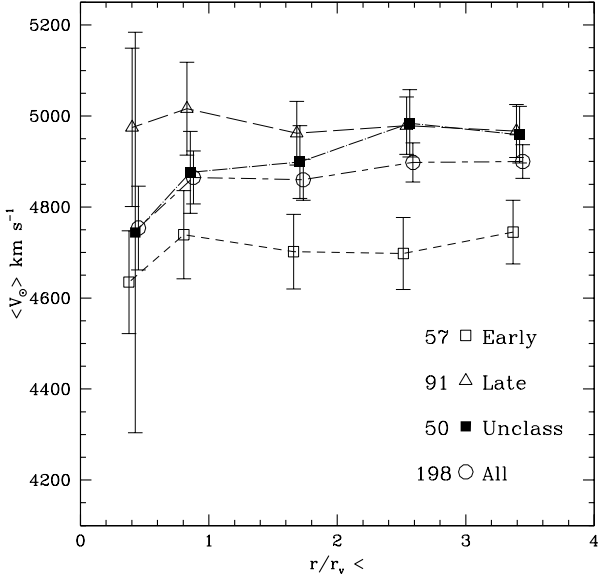


Fig. 10.— The integrated heliocentric velocity profiles for the entire catalog and several subpopulations. The points are artificially offset slightly from each other in r/r_v for clarity. The lines connecting the points are provided as a guide for the eye.

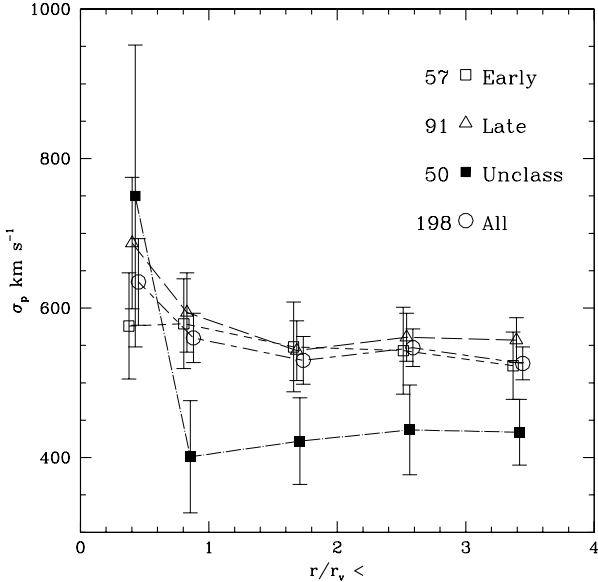


Fig. 11.— The integrated velocity dispersion profiles (VDPs) for the whole catalog and several subpopulations.

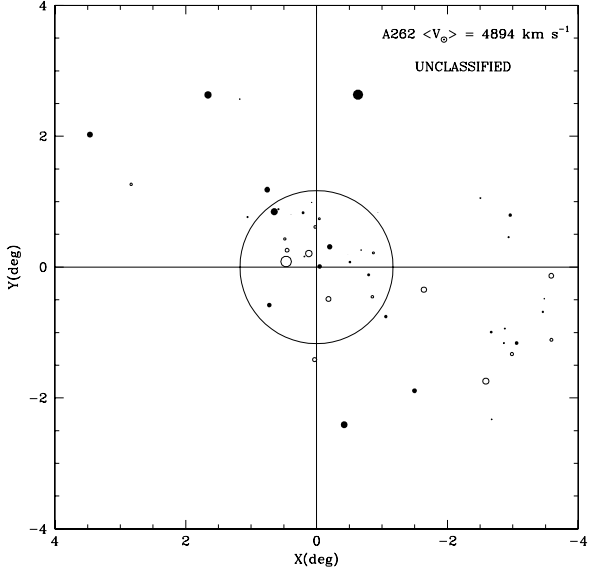


Fig. 12.— As for Figure 6, but for the unclassified galaxies.

dispersion is small because of its similarity to the early-type velocity dispersion. The unclassifieds lower the velocity dispersion only slightly due to their small number but, since they are on average 0.5 magnitudes fainter than the the classified galaxies, a survey to fainter magnitudes may reveal a greater impact. We discuss potential explanations for this phenomenon in Section 4.1.2.

3.3. The Anisotropy Parameter and the Virial Mass

The equation for determining the radial velocity dispersion and velocity anisotropy parameter from the projected dispersion is derived in Binney & Tremain (1987). Using the notation of DJF96,

$$I(b)\sigma_p^2(b) = 2 \int_b^\infty \left(1 - A \frac{b^2}{r^2}\right) \frac{\rho_{gal}(r)}{\sqrt{r^2 - b^2}} \sigma_r^2 r dr, \quad (1)$$

where b is the projected radial coordinate in the line-of-sight, σ_p is the projected velocity dispersion, $I(b)$ is the projected galaxy surface brightness, ρ_{gal} is the volume density of galaxies, σ_r is the radial velocity dispersion, and A the velocity anisotropy parameter $A = 1 - \sigma_\theta^2/\sigma_r^2$. Using a modified King profile for the galaxy density of $\rho_{gal} = \rho_0/(1 + r^2/r_{co}^2)^{3\beta_{fit,gal}/2}$, we can solve this equation for the curve $\sigma_r(A)$ that reproduces the measured σ_p . In practice, due to observational errors (primarily from σ_p), we find a region in the (σ_r, A) plane that satisfies the constraint. The optical core radius of the cluster galaxies is r_{co} . The core radius we used for the King profile was r_{co} determined in G98. The influence of a central cD galaxy can complicate the determination of this quantity, but the solution region is fairly insensitive to its value. We note that DJF96 simply

used the r_{cx} they determined from the *ROSAT* PSPC data, assuming that r_{co} and r_{cx} were equal.

We assumed that A and σ_r are independent of radius in the cluster. In order to further limit the solution set we impose a second constraint on σ_r and A which comes from the virial mass. The connection is in the form of the Jeans equation (Binney & Tremaine 1987)

$$M(r) = \frac{-\sigma_r^2 r}{G} \left(\frac{d \ln \rho_{gal}}{d \ln r} + \frac{d \ln \sigma_r^2}{d \ln r} + 2A \right). \quad (2)$$

DJF96 deduced σ_r and A using the X-ray determined virial mass in equation (2). Recently G98 has shown that excellent agreement can be obtained between X-ray and optical virial masses provided the optical virial masses are corrected for a surface energy term. This term accounts for the fact that observations are made out to a finite radius in the cluster. This correction has been emphasized in work on CNO clusters (Carlberg et al. 1996). The corrected optical virial mass can be expressed in terms of the standard virial mass according to the following equation (G98):

$$M_{cv} = M_v \left(1 - \frac{4\pi b^3 \rho_{gal}(b)}{\int_0^b 4\pi r^2 \rho_{gal}(r) dr} \left[\frac{\sigma_r(b)}{\sigma(< b)} \right]^2 \right), \quad (3)$$

where b is the boundary radius, $\rho_{gal}(b)$ the galaxy density evaluated at the boundary radius, $\sigma_r(b)$ the radial optical dispersion at the boundary radius, $\sigma^2(< b)$ the total optical dispersion ($= \sigma_r^2 + \sigma_\theta^2 + \sigma_\phi^2$) averaged out to the boundary radius. The uncorrected (or standard) virial mass is given by

$$M_v = \frac{3\sigma_p^2 r_v}{G}, \quad (4)$$

(G98, eq. [4]). Given the virial mass, equations (1) and (2) further constrain the solution for (σ_r, A) .

The values of (σ_r, A) so obtained will also provide a more accurate corrected virial mass. In quoting the virial mass below we refer to the total virial mass. As discussed by Carlberg et al. (1996) this is the mass contained within a radius of virialization defined by

$$\bar{\rho}(r_v)/\rho_c(z) = \frac{6}{(1+z)^2(1+\Omega_0 z)} \frac{\sigma_p^2}{H_0^2 r_v^2}, \quad (5)$$

where ρ_c is the critical mass density at redshift z and $\bar{\rho}(r_v)$ the mean density of the cluster out to the virial radius. Essentially all the virialized mass is accounted for if $\bar{\rho}(r_v)/\rho_c(z) = 200$ (Crone, Evrard, & Richstone 1994; Gunn & Gott 1972). G98 give an approximate method for determining the radius of virialization and Girardi et al. (1998b) give more exact iterative methods for determining the radius of virialization for different cosmological models. The virial mass we quote below is based on equation (5) which gives $r_v = 1.52$ Mpc ($1^{\circ}17$) and, for the low redshift of A262, differs by $< \sim 15\%$ from the r_v quoted in G98.

We used the following method to determine the range of orbital anisotropy, A , and radial velocity dispersion, σ_r , that produce consistency between equations (1) and (2). We used $\beta_{fit,gal} =$

0.73 from G98. We calculated the standard virial mass from equation (4) using the early-type σ_p . Then, from equation (1) we get a range of σ_r and A . We use these values to calculate the corrected virial mass from equation (3) as a function of A and use this in equation (2). Figure 13 plots the locus of σ_r , and A from equation (1) (dashed lines) and from equation (2) (solid lines) for the early-type galaxies in A262.

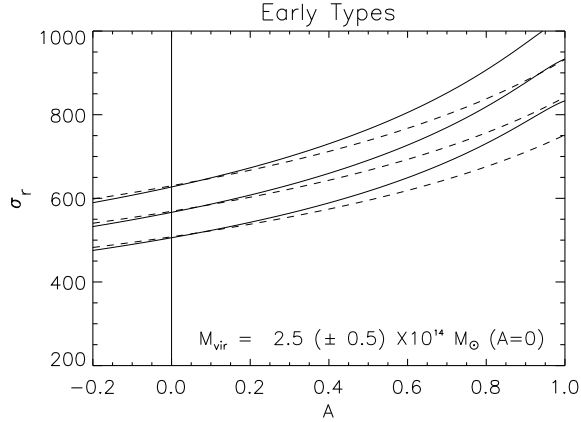


Fig. 13.— The range in radial velocity dispersion, σ_r , and anisotropy parameter, A , that reproduce the projected velocity dispersion, σ_p , are shown with dashed lines. Solid lines show the range in σ_r and A that reproduce the corrected virial mass, M_{cv} , from the stellar hydrodynamics equation (eq. [2]).

Unlike DJF96, we get complete overlap between these two distributions over all reasonable values of A (see below). We get a standard virial mass of $4.2 \times 10^{14} M_\odot$ which is slightly higher than the value in G98 due to our higher σ_p , however our corrected virial mass ($2.5 \times 10^{14} M_\odot$) is greater by $\sim 25\%$ (at $A = 0$). G98 used a statistical method for determining the value of A used in computing the mass correction. They divided all VDPs into three categories: centrally rising, flat, and centrally falling. They assigned A262 to the centrally rising category. With our larger catalog, we measure a flat VDP for the global population as well as each subpopulation. This accounts for the difference in our correction to the virial mass.

This analysis does not strongly constrain the range of A . In the following analysis we will take A to be zero, but will also consider the implications of a range of velocity anisotropies for the determination of β_{spec} .

4. DISCUSSION

4.1. The β -problem

The cluster gas is assumed to be described by the equation of hydrostatic equilibrium (Cavaliere & Fusco-Femiano 1976; Fabricant, Lecar, & Gorenstein 1980) and this leads to an expression for the cluster mass

$$M(r) = \frac{-kTr}{G\mu m_p} \left(\frac{d\ln \rho_{gas}}{d\ln r} + \frac{d\ln T}{d\ln r} \right), \quad (6)$$

where μm_p is the mean atomic weight of the gas and T the intra-cluster gas temperature. Equating the masses in equations (2) and (6) leads to an expression for the ratio of galaxy radial velocity dispersion to gas temperature (Bahcall & Lubin 1994). Using the notation of G98 with the modified King profiles and performing the logarithmic derivatives we obtain

$$\beta_{spec} \equiv \frac{\sigma_r^2}{kT/\mu m_p}, \quad (7)$$

$$\beta_{fit}^c \equiv \frac{\beta_{fit,gas}/\beta_{fit,gal}}{1 - 2A/3\beta_{fit,gal}}, \quad (8)$$

and

$$\beta_{spec} = \beta_{fit}^c. \quad (9)$$

In the case where the gas is isothermal and where the anisotropy parameter A is negligible we can identify β_{spec} with the ratio of cluster galaxy internal energy to gas kinetic energy. In this case β_{fit}^c just reduces to $\beta_{fit}^c = \beta_{fit} \equiv \beta_{fit,gas}/\beta_{fit,gal}$. The failure of β_{spec} to equal β_{fit}^c is the β -problem.

Using $\sigma_p = 569 \pm 61$ km s⁻¹, $T_x = 1.79_{-0.05}^{+0.08}$ KeV, and assuming $A = 0$ we get a β_{spec} of 1.13 ± 0.12 . With $\beta_{fit,gas} = 0.6 \pm 0.1$ and $\beta_{fit,gal}$ from G98 of 0.73 we get a β_{fit}^c of 0.82 ± 0.20 . Our analysis obtains values for β_{spec} and β_{fit}^c which are consistent to within statistical uncertainties; there is no β -problem. The β_{spec} obtained in this study is twice as high as that previously obtained (see Table 3). The β_{fit} we report is $\sim 50\%$ higher than prior determinations due to a new, lower $\beta_{fit,gal}$ for A262 reported in G98. As a check on the G98 value, we used our complete galaxy sample to calculate $\beta_{fit,gal}$. Our $\beta_{fit,gal}$ is statistically indistinguishable from the G98 value, but has a larger uncertainty. For the early type population we obtain a slightly higher $\beta_{fit,gal}$ but the errors are even larger for this very limited sample and our result is, within errors, consistent with G98. Therefore we have adopted the G98 number as the best current value of $\beta_{fit,gal}$.

Our conclusion that there is no β -problem in A262, while the same as that drawn by DJF96, is based on very different observational inputs and contains considerable subtleties. Moreover, although we both conclude that there is no β -problem, our higher β_{spec} has different implications (discussed below) for galaxy-gas feedback models. It is probably correct to discount the late-type galaxies in calculating β_{spec} but not because they have a different velocity dispersion from the early-type galaxies, as DJF96 suggested. Indeed, the late-type galaxies' velocity dispersion and VDP are statistically indistinguishable from the early-type galaxies and thus they do not affect

the calculation of β_{spec} at all. But, they clearly represent a distinct, unrelaxed cluster population. This manifests itself in their heliocentric velocity which differs from the early-type galaxies, their spatially extended distribution, and their non-Gaussian (but isothermal) velocity distribution. The unclassified population has an isothermal VDP but does have a statistically significant difference in velocity dispersion (see section 4.1.2). This population also has a peculiar heliocentric velocity. They should definitely be excluded from any calculation of β_{spec} in A262, but as a practical matter they are a small enough population (at least in A262) that they do not seriously affect the value of β_{spec} . Finally, the isothermal temperature profile of the galaxies, and lack of a significant X-ray temperature gradient (reported in DJF95) all argue against anomalies that might alter the conclusion that the β -problem does not exist in this cluster.

The basis for the difference in β_{spec} between this work and DJF96 is twofold. Firstly, our measurement of the velocity dispersion of the virialized early-type galaxies (569 km s^{-1}) is much higher than the 330 km s^{-1} (Moss & Dickens 1977) used by DJF96. The low value of velocity dispersion was based on only 9 elliptical galaxies, which shows the importance of obtaining a statistically large sample for analysis of subpopulations within a cluster. Secondly, the X-ray temperature we determined from the ASCA data is higher than that determined by DJF96 from the ROSAT data. It is, however, the large difference in velocity dispersion between our samples that dominates the difference in β_{spec} .

4.1.1. Implications for the Dynamics of A262

The solution to the β -problem presented here, at twice the previously reported β_{spec} , has implications for the general state of A262. We have quoted a β_{spec} solution for the assumption that the velocity anisotropy parameter $A = 0$. The flat VDPs that we measure for the early-type galaxy population suggest $A = 0$ is a plausible supposition. However, as Figure 13 indicates, the radial velocity and A are not well-constrained by either the Jeans equation method or the line-of-sight velocity dispersion method. Indeed, these two approaches produce virtually identical constraints on radial velocity and A . The two methods should give the same constraints but often do not. Our excellent agreement results from using the corrected optical virial mass as determined by the method of Carlberg et al. (1996) (Equation 3) in the Jeans equation and then iterating to demand self-consistency between the Jeans equation and the corrected virial mass equation. With this procedure the Jeans equation is determining the correct σ_r and A relation, just as the line-of-sight velocity dispersion method does (Equation 1). Indeed, it is precisely because we are properly utilizing the Jeans equation that it provides no extra information about the relation between σ_r and A beyond that obtained from the line-of-sight velocity dispersion equation. However, the excellent agreement between these determinations does tell us that the early type galaxy population used in the analysis is well-virialized.

Aside from assuming the plausible $A = 0$, we can draw a coarse conclusion about the maximum value of A in this cluster. The very largest values of β_{spec} , measured for clusters in which there

is minimal substructure, is ~ 1.3 (BMM95). For our nominal curve of $\sigma_r(A)$, this would imply a rough upper limit of $A < \sim 0.25$. This is entirely consistent with the work of van der Marel et al. (1999) who found a range of A from -0.05 to 0.26 for their cluster ensemble derived from 16 clusters in the CNOC1 survey.

The higher β_{spec} we have found for this cluster is most relevant to discussions of galaxy-gas feedback and entropy-floor models. If $A = 0$, then our β_{spec} for A262 is consistent with the mean value of β_{spec} (0.91, see Table 3) determined for several large cluster samples which either had substructure corrections applied or involved luminous X-ray selected systems claimed to be less likely to have substructure. A larger β_{spec} has been obtained from a cluster sample of more heterogeneous morphology (1.14, see Table 3). Our 90% lower limit on β_{spec} is 0.95 for $A = 0$. Assuming that $A = -0.05$, the lowest A obtained in the van der Marel et. al. sample, the lower limit on β_{spec} is 0.92. These lower limits both imply that A262 could have at most a $\sim 5\%$ enhancement of gas temperature with respect to galaxy temperature.

This (at most) mild overheating of gas with respect to galaxies we obtain for A262 is in marked contrast to the factor of 2 overheating inferred from the β_{spec} of DJF96. It is interesting to place our results in the context of models for galaxy-gas feedback through winds in early galaxies or through dynamical friction in galaxies. Several authors have suggested a correlation between cluster velocity dispersion and gas temperature steeper than predicted by the virial equation (see BMM95 and references therein) but the scatter in the cluster data is large. Nevertheless, a steeper relation between velocity dispersion and gas temperature (effectively a temperature-dependent β_{spec}) can be argued as resulting from winds injecting energy into the cluster or from dynamic friction of galaxies in the cluster.

The simulations of Metzler & Evrard (1994) as presented in BMM95, which include the dark matter, galaxies and winds, offer support for the contention that β_{spec} is temperature dependent. Their simulations would predict, given the temperature of A262, that $\beta_{spec} \sim 0.6$. This is substantially lower than the lower limit we have derived for β_{spec} . The simulations suggest that a cluster would need a $T > \sim 3$ KeV to obtain the type of β_{spec} we measure.

There are possible problems with this analysis. As pointed out by BMM95, to obtain this T-dependent β_{spec} , the simulations required the use of much greater wind luminosities for early galaxies than are realistic. The assumption that galaxies can be modeled as collisionless particles is also questionable (Frenk et al. 1996). Since A262 gives results consistent in all respects with a well-relaxed system suffering from minimal substructure complications in the early-type galaxy population, the discrepancy with the predictions of wind models are hard to ignore. While the analysis in BMM95 lends support to the idea of a T-dependent β_{spec} , it is not clear on the whole whether that translates into support for the galaxy wind models. Clearly, further work is warranted on models attempting to predict this velocity dispersion-temperature correlation.

We have demonstrated there is no β -problem in A262. Our solution is consistent with Edge & Stewart (1991b), who suggested the β -problem is likely associated with improper determinations

of velocity dispersion, as emphasized in BMM95. Alternately, it should be pointed out that Bahcall and Lubin (1994) have proposed that the beta-problem vanishes in general when one utilizes the proper average net galaxy density around clusters, as determined from galaxy-cluster cross-correlation. This approach provides a shallower dependence on ρ_{gas} ($\rho_{gas} \propto r^{-2.2}$, Schombert 1988; Bahcall 1977) than the canonical King approximation ($\rho_{gas} \propto r^{-3}$). It produces a value of β_{fit} which is in better agreement with β_{spec} when both are suitably averaged over an ensemble of clusters. The agreement is purported to hold even in the case of non-isothermal clusters (cf. Eq. 6). This is not in agreement with BMM95, since their solution requires only gravitational energy to feed the cluster processes. It is possible that all these works suffer from the shortcoming of relying on ensembles of clusters to draw conclusions about β_{spec} . Additional insights should be obtained as more individual clusters are scrutinized with detailed optical and X-ray studies to form a comprehensive picture of their interactions.

4.1.2. β_{spec} , The Unclassified Population and Velocity Fields

Two unvirialized galaxy subpopulations have been identified in A262. The late-type galaxies have a mean velocity dispersion averaged over the virial radius and a VDP which are statistically the same as those for the early-type galaxies. They are dynamically distinct in that they show a much less concentrated spatial distribution and have a significant velocity offset with respect to the early-type galaxies. The unclassified galaxies are distinct from the early-type galaxies for these same two reasons, but in addition have a significantly lower (but flat) VDP. Based on their appearance in Figure 10, the unclassifieds are a mix of early and late-type galaxies in the central bin and become more dominated by the late-type galaxies as r increases.

The most peculiar aspect of the unclassified galaxies is their low VDP. If they represent a more recent infalling wave of galaxies whose peculiar motion is along the plane of the sky, this would explain their lower velocity dispersion. They could also be a ‘local field’ population originating from the Pisces-Perseus supercluster ridge which is coincident with the plane of the sky. These low-luminosity and presumably low-mass galaxies could have been ejected from other clusters in the supercluster ridge through mass segregation. In this description, the early-type galaxies trace the cluster potential well, the late-type (classified) galaxies have infallen, but not yet equilibrated with the cluster potential, and the unclassified galaxies trace the background supercluster at a constant velocity offset and lower velocity dispersion. Edge & Stewart (1991b) have previously discussed how such field galaxies, if not properly accounted for, may contribute to the existence of a β -problem.

4.1.3. The Virial Mass of A262

Using the optical and X-ray analyses we can compare the virial masses determined by the two methods. The equation of hydrostatic equilibrium (see DJF95, Eq. 3) yields an X-ray mass of $M_x = 1.9 \pm 0.3 \times 10^{14} M_\odot$. From our velocity dispersion within the virial radius, assuming an anisotropy parameter of $A = 0$ and using the correction of Carlberg et al. (1996), we derive an optical mass of $M_{opt} = 2.5 \pm 0.5 \times 10^{14} M_\odot$. The agreement between the two determinations is quite good (25%) and well within the statistical errors. G98 reported that optical and X-ray determined virial masses for a large ensemble of clusters could on average be brought into a statistical agreement of $\sim 30\%$ if the optical virial masses were corrected for the surface term in the virial equation as prescribed in Carlberg et al. (1996). We have shown here that the same techniques, employed on individual clusters in which a virialized galaxy subpopulation can be identified, also yields good agreement between X-ray and optical masses.

4.2. Entropy Floor Models, and the $L_x - T$ Relation

DJF96 concluded that the gas temperature in A262 was a factor of 2 higher than the galaxy temperature. A high (but not that high) gas temperature relative to the galaxy temperature fits comfortably into a larger theoretical framework for understanding clusters.

Observations of low richness class clusters, including A262, show that the cluster entropy, when plotted as a function of radius normalized to the cluster virial radius, tends to be flat in the interior regions, and increases sharply at larger radii. This is roughly consistent with predictions of the “entropy floor” model (Evrard & Henry 1991; DJF96). In the entropy floor model there is assumed to be substantial preheating of the proto-intracluster medium at high redshift. This heating leads to an adiabatic cluster inner region, and increasing entropy in the outer regions due to shock heating of infalling gas. The entropy floor model not only makes a specific prediction about the entropy as a function of cluster radius (normalized to the virial radius), but it also makes a definite prediction about the cluster $L_x - T$ relation. Recent observational data on several sets of clusters (Henry 1997; Arnaud & Evrard 1999) suggest an $L_x - T$ relation for the entropy floor model which is roughly consistent with the observed slope of the $L_x - T$ relation. The entropy floor model also correctly predicts the observed minimal (or no) evolution of the $L_x - T$ relation with redshift. More complex models also make predictions which are in accord with current data, including semi-analytic models in which the $L_x - T$ slope changes with cluster temperature (Cavaliere, Menci, & Tozzi 1997), the punctuated equilibrium model (Cavaliere, Menci, & Tozzi 1999) and certain wind models (Metzler & Evrard 1994).

The entropy floor model does appear to provide agreement with the radial entropy profile in A262 as determined by DJF96. The flatter gas profile is also in accord with models in which there is early heating of the gas. These models also predict substantially higher gas than galaxy temperatures in poor richness class clusters. The higher gas temperature is expected because

energy input from the galaxies into the gas is roughly independent of the richness class, leading to disproportionate heating in the low richness class clusters. Our β_{spec} range in A262 is consistent with no overheating of gas with respect to galaxies, or a very mild overheating ($< \sim 10\%$). This is in accord with observations of other clusters with minimal substructure. Given the X-ray temperature of A262, one would estimate from the model results presented in BMM95 that the β_{spec} of A262 would be ~ 0.7 . The error on this quantity could be substantial, so it is difficult to ascertain whether or not there is a statistically significant disagreement with our results. It is possible that the flat entropy profile of A262 is commensurate with very mild overheating of gas with respect to galaxies, rather than the gross overheating argued for by DJF96.

The fact that galaxy-gas feedback models predict the entropy profile, but may be inconsistent with typical β_{spec} values near unity – indicative of either non-existent or mild overheating of the gas – is a conundrum. This conundrum prompted us to look into the entropy-floor model in more detail, independent of the A262 study. We have found significant new support for the model in that it provides a theoretical basis for understanding a recently discovered empirical relationship between r_{cx} , r_v , and $\beta_{fit,gas}$ for a given cluster (NA99). In NA99 a quadratic correlation was discovered between $\beta_{fit,gas}$ and r_{cx}/r_v . A two parameter empirical fit was utilized which involved an overall normalization and a cluster scale length. As explained below we have produced a fit to the correlation using the data set of NA99, obtaining it at higher statistical significance and without removing any select clusters (as was done in NA99). Moreover the entropy floor model requires only one, not two free parameters.

To obtain this correlation we used the entropy-floor model relation as given in Evrard & Henry (1991) for the central gas density scaling with temperature, $\rho_{gas}(0) \propto T^{1/(\gamma-1)}$, along with an expression for the virial density at radius r_v ,

$$\bar{\rho}_v(z, \Omega_0) = \frac{3}{r_v^3} \int_0^{r_v} f_b^{-1} \frac{\rho_{gas}(0)}{[1 + (r/r_{cx})^2]^{3\beta_{fit,gas}/2}} r^2 dr, \quad (10)$$

where r_{cx} is the core radius and f_b the baryonic mass fraction. This relation can be manipulated to obtain a relation between r_{cx} , r_v , and $\beta_{fit,gas}$:

$$\left(\frac{r_{cx}}{r_0}\right)^3 \int_0^{r_v/r_{cx}} \frac{y^2}{(1+y^2)^{3\beta_{fit,gas}/2}} dy = 1. \quad (11)$$

In this equation, r_0 is a scale length which depends on the thermodynamics of the energy input and cosmological model (largely irrelevant for the NA99 sample which was at low redshift). Equation (11) provides a definite relation between the quantities of relevance, and the only fit parameter, the scale length. In addition, NA99 were unable to definitively conclude whether the correlation they deduced was simply between $\beta_{fit,gas}$ and r_{cx} or r_{cx}/r_v . The entropy-floor model clearly indicates that the relationship is between $\beta_{fit,gas}$ and the radius ratio. We have compared the predictions of the entropy-floor model in this case directly with the cluster data set of NA99. We have followed exactly their procedure for assessing the significance of the correlation. In particular, we used χ^2 fitting to assess the significance of the results and we increased the error bars on the observational

quantities in the manner prescribed by NA99 to account for the highly correlated errors between r_{cx} and $\beta_{fit,gas}$. Figure 14 presents the data overlaid with the model predictions. Our best fits indicate that the model and data agree at better than the 99% confidence level. This agreement is much better than the $\sim 65\%$ confidence level obtained in NA99. Moreover, we used all the cluster data and one less free parameter in our fit. Even the $\sim 65\%$ confidence level of NA99 was only obtained when 4 clusters were dropped from the data set. Our relation is more complicated than just a quadratic relation, but it also rests on a firmer theoretical foundation. The scale length r_0 that we derive is, within fitting uncertainties, comparable to that of the 2 parameter fit of NA99.

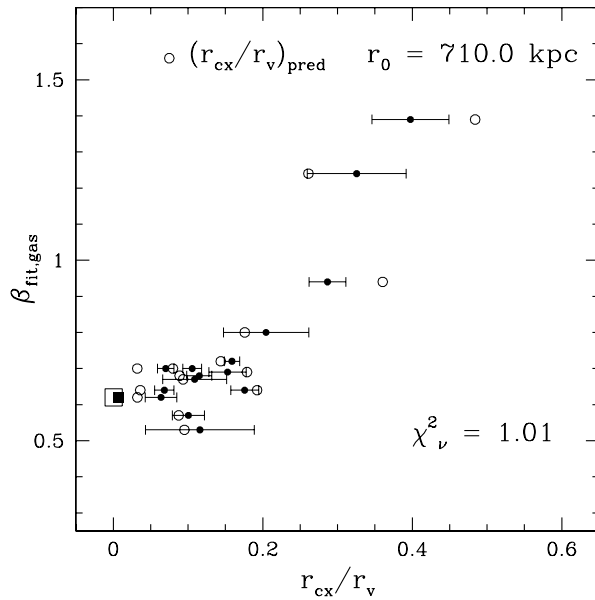


Fig. 14.— r_{cx}/r_v vs $\beta_{fit,gas}$ from NA99 (filled circles) and predicted from the entropy floor model with one free parameter (open circles). The error-bars plotted are unscaled. The observed value for A262 is indicated with a filled square and its predicted value with the open square.

The NA99 sample consists of fairly high temperature (> 3 KeV) clusters. Thus, the assumption of the entropy-floor model that the luminosity is dominated by bremsstrahlung and not line emission is certainly valid. However, the sample of NA99 does not constitute a homogeneous class of clusters and one might expect more detailed fitting, perhaps with different scale lengths, to be required. NA99 pointed out the need for a cluster sample covering a wider range of temperature and richness class. Viewed in this fashion, the above derived relation within the entropy-floor model seems very encouraging and surprisingly robust. NA99 argue that the regularity they find in gas density profiles outside the cluster cores, independent of temperature, is evidence that non-gravitational heating is negligible in their sample. They point out that this is consistent with the recent work of Ponman, Cannon & Navarro (1999), who demonstrated that lower T clusters have higher entropies. However the entropy-floor model assumes a non-gravitational heating effect that decreases with increasing temperature. The fact that equation (11) fits the relation between $\beta_{fit,gas}$, r_{cx} and r_v fairly well,

regardless of temperature, validates the idea of substantial early heating of the proto-intracluster medium (as do flat entropy profiles in low richness class clusters). The cluster sample does not go to low enough temperatures to determine whether or not the derived relation will also hold for lower temperature, lower richness class clusters. For these clusters the heating is relatively stronger but this effect is perhaps offset by the increased dominance of line emission cooling compared to bremsstrahlung. Nevertheless we show the A262 data point in Figure 14, and the prediction of equation (11). The agreement is good.

5. CONCLUSIONS

- 1) The early- and late-type galaxy populations in A262 both have isothermal VDPs. There is no evidence that the early-type galaxies have a much lower velocity dispersion than the late-type galaxies. The velocity dispersion of the early populations is 569 km s^{-1} , much higher than the 330 km s^{-1} used in a previous solution to the β -problem, and based on a sample of only 9 elliptical galaxies. The main population of late-type galaxies do differ from the early-type galaxies in having a non-Gaussian velocity dispersion, a different heliocentric velocity and a spatially extended profile.
- 2) The β_{spec} derived for A262 on the basis of improved velocity dispersion and X-ray gas temperature measurements is 1.13 ± 0.12 , consistent with the global mean for clusters with minimal substructure. The gas temperature is not a factor of 2 higher than the galaxy temperature, as previous measurements had suggested, but rather comparable. Therefore there is no evidence for strong galaxy-gas feedback. The new observations may be in better accord with models since they do not require artificially high wind velocities or strong dynamical friction to produce a dramatic factor of 2 difference in the gas and galaxy temperature.
- 3) To within the observational uncertainties there is no β -problem in A262. For a velocity anisotropy parameter of $A = 0$ the galaxy temperature is slightly higher than the gas temperature ($\sim 10\%$), although within the observational uncertainties the galaxy temperature could be slightly less than the gas temperature by an almost comparable amount ($\sim 5\%$). Even for reasonable anisotropies the best fit gas and galaxy temperature are also approximately the same. The important point is that the β -problem is solved in a fashion which does not require significant gas heating with respect to galaxies. The derived β_{spec} is in much better agreement with that obtained from a statistical analysis of β_{spec} for either X-ray selected clusters or optically selected clusters with substructure corrections applied.
- 4) We have discovered a population of unclassified, low luminosity galaxies with an isothermal VDP but with a much lower velocity dispersion than the standard cluster galaxy populations. These galaxies have a roughly uniform spatial distribution unlike the main virialized early-type galaxy population, which is centrally concentrated. They may represent a second population of infalling late-type galaxies or a ‘local field’ population which distinguish themselves from the primary population only by their smaller velocity dispersion. They are probably associated with the

Pisces-Perseus ridge in which A262 is located.

5) We have used the entropy-floor model to develop a relation that explains the recently discovered correlation between cluster $\beta_{fit,gas}$ and the ratio of r_x to r_v . The correlation can be explained with a one parameter fit, rather than the two parameter empirical fits previously employed. This provides additional support for the entropy-floor model in addition to its ability to approximately predict the $L_x - T$ relation and the fact that flat entropy profiles are found in low richness class clusters.

We acknowledge useful discussions with Jacqueline vanGorkom and David J. Helfand. We also acknowledge the useful comments from the anonymous referee. Optical observations were made using the Automated Multi-Object Spectrometer at the University of California's Lick Observatory. This research has made use of data obtained from the High Energy Astrophysics Science Archive Research Center (HEASARC), provided by NASA's Goddard Space Flight Center. We have also used NASA's Extra-galactic Database, ADS Abstract Service, and the Digitized Sky Survey at STScI.

REFERENCES

Arnaud, K.A. 1996, Astronomical Data Analysis Software & Systems V, eds. Jacoby G. & Barnes J., p17, ASP Conf. Series volume 101

Arnaud, M. & Evrard, A. E. 1999, MNRAS, 305, 631

Bahcall, N. A. 1977, ARA&A, 15, 505

Bahcall, N. A., & Lubin, L. M. 1994, ApJ, 426, 513

Beers, T. C., Flynn, K., & Gebhardt, K. 1990, AJ, 100, 32

Binney, J., & Tremain, S. 1987, Galactic Dynamics (Princeton: Princeton Univ. Press)

Bird, C. M. & Beers, T. C. 1993, AJ, 105, 1596

Bird, C. M., Mushotzky, R. F., & Metzler, C. A. 1995, ApJ, 453, 40 (BMM95)

Carlberg, R. G., Yee, H. K. C., Ellingson, E., Abraham, R., Gravel, P., Morris, S., & Pritchett, C. J. 1996 ApJ, 462, 32

Cavaliere, A., & Fusco-Femiano, R. 1976, A&A, 49, 137

Cavaliere, A., Menci, N., & Tozzi, P. 1997, ApJ, 484, L21

Cavaliere, A., Menci, N., & Tozzi, P. 1999, MNRAS, 308, 599

Crone, M. M., Evrard, A. E., & Richstone, D. O. 1994, *ApJ*, 434, 402

Craig, W. W., Cook, K. H., Hailey, C. J., Brodie, J. P. 1993, in Gray, P. M., ed, *Proceedings of the second “Fibre Optics in Astronomy” Conference*, ASP, 37, 106

David, L. P., Slyz, A., Jones, C., Forman, W., & Vrtilek, S. D. 1993, *ApJ*, 412, 479

David, L. P., Jones, C., & Forman, W. 1995, *ApJ*, 445, 578 (DJF95)

David, L. P., Jones, C., & Forman, W. (1996, *ApJ*, 473, 692 (DJF96)

Edge, A. C., & Stewart, G. C. 1991, *MNRAS*, 252, 414

Edge, A. C., & Stewart, G. C. 1991, *MNRAS*, 252, 428

Evrard, A. E., & Henry, J. P. 1991, *ApJ*, 383, 95

Fabricant, D., Lecar, M., & Gorenstein, P. 1980, *ApJ*, 241, 552

Frenk, C. S., Evrard, A. E., White, S. D. M., & Summers, F. J. 1996, *ApJ*, 472, 460

Girardi, M., Escalera, E., Fadda, D., Giuricin, G., Mardirossian, F., & Mezzetti, M. 1997, *ApJ*, 482, 41

Girardi, M., Giuricin, G., Mardirossian, F., Mezzetti, M., & Boschin, W. 1998a, *ApJ*, 505, 74 (G98)

Girardi, M., Borgani, S., Giuricin, G., Mardirossian, F., & Mezzetti, M. 1998b, *ApJ*, 506, 45

Gunn, J. E., & Gott, J. R., III 1972, *ApJ*, 176, 1

Henry, J. P. 1997, *ApJ*, 489, L1

Huchra, J. P. 1999, CfA Redshift Catalog, unpublished

Jacoby, G. H., Hunter, D. A., & Christian, C. A. 1984, *ApJS*, 56, 257

Jedrzejewsky, R. I. 1987, *MNRAS*, 226, 747

Kurtz, M. J., & Mink, D. J. 1998, *PASP*, 110, 934

Lubin, L. M. & Bahcall, N. A. 1993, *ApJ*, 415, L17

Menci, N., & Fusco-Femiano, R. 1986, *ApJ*, 472, 46

Metzler, C. A., & Evrard, A. E. 1994, *ApJ*, 437, 564

Moss, C., & Dickens, R. J. 1977, *MNRAS*, 178, 701

Press, W. H., & Schechter, P. 1974, *ApJ*, 187, 425

Neumann, D. M., & Arnaud, M. 1999, A&A, 348, 711

Ponman, T. J., Cannon, D. B., & Navarro, J. F. 1999, Nature, 397, 135

Sakai, S. , Giovanelli, R., & Wegner, G. 1994, AJ, 108, 33

Sarazin, C. L. 1986, Rev. Mod. Phys., 58, 1

Schombert, J. M. 1988, ApJ, 328, 475

Scoggio, M., Giovanelli, R., & Haynes, M. P. 1998, AJ, 116, 2738 (SGH98)

Tody, D. 1986, Proc. SPIE, 627, 733

Tonry, J., & Davis, M. 1979, AJ, 84, 1511

van der Marel, R. P., Magorrian, J., Carlberg, R. G., Yee, H. K. C., & Ellingson, E. AJ, submitted, astro-ph/9910494

Yahil, A. & Vidal, N. V. 1977, ApJ, 214, 347

Table 1. New Velocities for A262^a.

N	ID	RA(J2000) h m s	Dec(J2000) ° ' "	cz km s ⁻¹	R	N lines	Type	Ref
1	-	01 50 33.40	+36 16 42.5	4912 ± 64	3.5	-	-2	
2	-	01 50 45.83	+36 12 31.5	9750 ± 39	3.6	-	-7	
3	IC 1732	01 50 47.89	+35 55 57.7	4798 ± 16	15.4	-	-2	CFA
4	-	01 50 51.78	+35 40 33.6	4817 ± 37	3.4	-	-2	
5	-	01 50 56.76	+36 08 41.0	3280 ± 51	2.7	-	-2	
6	-	01 51 26.56	+35 56 03.1	7799 ± 17	7.9	-	-7	
7	01485+3549	01 51 29.20	+36 03 57.5	5311 ± 05	5.8	6	5	CFA
8	A0148+3537	01 51 32.48	+35 52 32.2	4706 ± 25	4.3	-	-7	CFA
9	-	01 51 51.70	+36 15 01.8	3755 ± 33	5.4	-	-7	
10	A0148+3614	01 51 53.26	+36 29 08.3	4297 ± 18	3.7	-	20	CFA
11	NGC 700	01 52 12.74	+36 05 50.6	4255 ± 15	6.0	-	-2	CFA,SGH98
12	01493+3547	01 52 16.86	+36 02 12.2	4590 ± 13	9.0	-	-2	CFA,SGH98
13	UGC 1339	01 52 24.85	+35 51 23.0	4059 ± 10	17.2	-	-2	CFA
14	A0149+3615	01 52 28.03	+36 29 52.3	4407 ± 29	4.3	-	20	CFA
15	-	01 52 34.14	+36 03 09.5	2820 ± 31	3.9	-	-7	
16	01497+3615	01 52 34.73	+36 30 03.0	4170 ± 09	4.7	-	1	CFA
17	NGC 704A	01 52 37.71	+36 07 36.6	4728 ± 06	6.8	-	-2	CFA
18	NGC 709	01 52 50.66	+36 13 24.3	3781 ± 37	8.0	-	-2	CFA
19	NGC 710	01 52 53.94	+36 03 11.5	6132 ± 07	4.7	5	5	CFA
20	01500+3615	01 52 57.46	+36 30 46.2	5020 ± 09	4.9	-	3	CFA
21	A0150+3551B	01 52 59.59	+36 06 26.1	4025 ± 24	6.4	-	-7	CFA
22	-	01 53 04.07	+35 51 01.7	10876 ± 05	4.2	5	20	
23	-	01 53 04.92	+36 35 24.4	5462 ± 27	5.0	-	-2	
24	A0150+3606A	01 53 09.47	+36 20 44.6	5045 ± 23	4.8	-	20	CFA
25	01504+3546	01 53 23.82	+36 00 43.8	4820 ± 18	6.4	-	-5	CFA,SGH98
26	NGC 714	01 53 29.66	+36 13 16.6	4418 ± 16	5.4	-	0	CFA,SGH98
27	01509+3606	01 53 50.15	+36 21 01.1	4156 ± 06	3.0	3	-5	CFA,SGH98
28	-	01 53 51.49	+36 12 11.9	4295 ± 36	3.7	-	-7	
29	01513+3540	01 54 11.32	+35 55 20.5	4285 ± 18	4.9	5	1	CFA
30	-	01 54 47.50	+36 01 20.4	4259 ± 104	4.4	-	-7	
31	-	01 54 51.54	+35 57 32.4	2859 ± 23	4.9	-	-2	
32	-	01 54 54.28	+36 01 57.8	3545 ± 19	6.7	-	-2	
33	A0151+3537	01 54 55.05	+35 52 28.2	4886 ± 47	4.1	4	20	CFA

^a Column 1 gives our sequential ID, column 2 gives the published ID, if available, column 3 and 4 give the coordinates, column 5 gives the heliocentric velocity with 1σ error, column 6 gives the Tonry & Davis (1979) R value for the absorption-line galaxies, column 7 gives the number of emission lines fit for emission-line galaxies, column 8 gives the morphological type code (Huchra 1999), and column 9 gives the reference for previously published observations.

Table 2. Derived Optical Properties out to r_v ($1^\circ 17$)^a

Pop	N_{gal}	cz km s $^{-1}$	σ_p km s $^{-1}$	TI	a-test	W-test
All	101	4869 ± 55	548 ± 36	0.967	0.804	0.983 (66%)
Early	38	4736 ± 94	569 ± 61	0.973	0.799	0.985 (92%)
Late	40	4993 ± 92	572 ± 50	0.861	0.832	0.962 (28%)
Unclass	23	4894 ± 90	418 ± 74	1.036	0.766	0.978 (85%)

^a Column 1 gives the population type, column 2 gives the number of galaxies in the sample, column 3 gives the average heliocentric velocity with 1σ error, column 4 gives the velocity dispersion with 1σ error, column 5 gives the scaled tail index, column 6 gives the a-test statistic, column 7 gives the W-test statistic with percent probability in parenthesis.

Table 3. Comparison of β s.

Source	β_{spec}	β_{fit}	$\beta_{fit,gas}$	$\beta_{fit,gal}$
A262				
DJF96	0.51	0.53	0.53	1.0
This work	1.13 ± 0.12	0.82 ± 0.1	0.6 ± 0.1	0.73 ^a
Statistical β_{spec}				
BMM95 ^b	1.14 ± 0.08			
ES91 ^c	$0.91^{+0.11}_{-0.13}$			

^afrom G98

^bcalculated from Table 1 in Lubin & Bahcall (1993)

^cEdge & Stewart (1991b)